Antiviral drug ganciclovir is a potent inhibitor of microglial proliferation and neuroinflammation

Zhaoqing Ding,[1,2] Vidhu Mathur,[1] Peggy P. Ho,[1] Michelle L. James,[3] Kurt M. Lucin,[1] Aileen Hoehne,[3] Haitham Alabsi,[1] Sanjiv S. Gambhir,[3] Lawrence Steinman,[1,2] Jian Luo,[1,4] and Tony Wyss-Coray[1,2,4]

[1]Department of Neurology and Neurological Sciences; [2]Immunology Interdepartmental Program; and [3]Molecular Imaging Program at Stanford, Department of Radiology; Stanford University School of Medicine, Stanford, CA 94305
[4]Center for Tissue Regeneration, Repair, and Restoration, Veterans Affairs Palo Alto Health Care System, Palo Alto, CA 94304

Aberrant microglial responses contribute to neuroinflammation in many neurodegenerative diseases, but no current therapies target pathogenic microglia. We discovered unexpectedly that the antiviral drug ganciclovir (GCV) inhibits the proliferation of microglia in experimental autoimmune encephalomyelitis (EAE), a mouse model for multiple sclerosis (MS), as well as in kainic acid–induced excitotoxicity. In EAE, GCV largely prevented infiltration of T lymphocytes into the central nervous system (CNS) and drastically reduced disease incidence and severity when delivered before the onset of disease. In contrast, GCV treatment had minimal effects on peripheral leukocyte distribution in EAE and did not inhibit generation of antibodies after immunization with ovalbumin. Additionally, a radiolabeled analogue of penciclovir, [^{18}F]FHBG, which is similar in structure to GCV, was retained in areas of CNS inflammation in EAE, but not in naive control mice, consistent with the observed therapeutic effects. Our experiments suggest GCV may have beneficial effects in the CNS beyond its antiviral properties.

CORRESPONDENCE
Tony Wyss-Coray:
twc@stanford.edu
OR
Jian Luo:
jianl@stanford.edu

Abbreviations used: CNS, central nervous system; d.p.i., day postimmunization; EAE, experimental autoimmune encephalomyelitis; GCV, ganciclovir; GFAP, glial fibrillary acidic protein; MS, multiple sclerosis; PET, positron emission tomography; tk, thymidine kinase.

Microglia are the resident myeloid phagocytes of the central nervous system (CNS), where they fulfill important functions in normal physiology and in the response to injury or disease (Saijo and Glass, 2011). Activated microglia, which are a hallmark of neuroinflammation, may contribute to CNS damage and chronic neurodegeneration through the release of harmful cytokines, reactive oxygen species, or uncontrolled phagocytosis (Lucin and Wyss-Coray, 2009). For example, microglia contribute to neurodegeneration in superoxide dismutase 1 transgenic mouse models for amyotrophic lateral sclerosis (Boillée et al., 2006), and microglia lacking fractalkine receptor, CX3CR1, promote protein aggregation and disease in tau transgenic models of Alzheimer's disease and related tauopathies (Bhaskar et al., 2010). Interestingly, microglial activation appears indicative of disease activity in multiple sclerosis (MS) patients based on positron emission tomography (PET) imaging with a ligand that binds to peripheral benzodiazepine receptors on activated microglia (Banati et al., 2000). These observations raise the possibility that selective inhibition of microglia may be beneficial in certain CNS disorders with a neuroinflammatory component, but today no treatments targeting aberrantly activated microglia are available to test this hypothesis.

Ganciclovir (GCV) is a prodrug nucleoside analogue, which in its canonical function requires bioactivation by viral thymidine kinase (tk) from viruses of the *Herpesviridae* family, including cytomegalovirus, Epstein-Barr virus, or HSV (Matthews and Boehme, 1988; Faulds and Heel, 1990). GCV was developed in the 1970s as an antiviral treatment and is currently used clinically to control cytomegalovirus and other viral infections. More recently, it has been used in research studies for the targeted deletion of cells genetically engineered to express HSV tk (HSV*tk*; Culver et al., 1992; Fillat et al., 2003) or for imaging tk expressing transgenic cells using modified, radiolabeled GCV analogues (Min et al., 2003). Besides its potent effects on

The Rockefeller University Press $30.00
J. Exp. Med. 2014 Vol. 211 No. 2 189-198
www.jem.org/cgi/doi/10.1084/jem.20120696

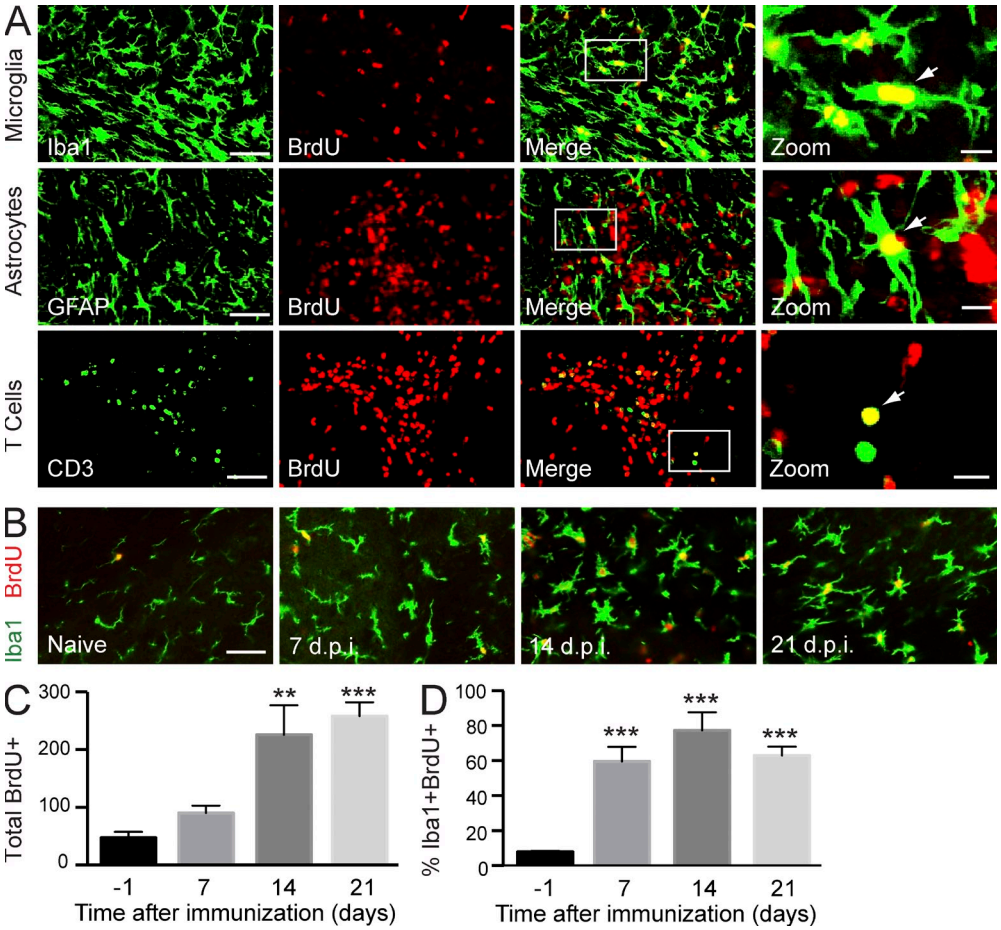

Figure 1. Neuroinflammation in EAE is characterized by expansion of proliferating microglia/macrophages. 8–12-wk-old mice were immunized subcutaneously with 200 µg MOG_{35-55} peptide emulsified in CFA and received an i.v. injection of 400 ng pertussis toxin at the time of immunization and 48 h later. Mice were sacrificed at 21 d.p.i.; BrdU was given three consecutive days before sacrifice. (A) Cerebellar sections from 21 d.p.i. EAE mice were double immunolabeled for BrdU (red) and cell type–specific markers (green) Iba1 (microglia/macrophages), GFAP (astrocytes), and CD3 (T cells). Images were taken outside of inflammatory foci to show individual cells. Far right column shows high magnifications of the white boxed areas. The proliferating cells appear yellow (arrows) after superimposition of single color images. (B–D) Cerebellar sections from naive (day −1) and EAE (7, 14, and 21 d.p.i.) mice were double immunolabeled for $BrdU^+$ (red) and $Iba1^+$ (green; B). Quantification of total $BrdU^+$ cells (C) and percentage of $Iba1^+BrdU^+$ (D) in the cerebella. Bar graphs represent the mean of three to five sections from an individual mouse and SEM (n = 5–10 mice/group). **, $P < 0.01$; ***, $P < 0.001$ by ANOVA and Dunnett's test. The experiments were independently performed three times. Bars: (A [left] and B) 50 µm; (A, right) 10 µm.

viral replication, GCV has been described to inhibit proliferation of uninfected cells, most notably of bone marrow cells, at concentrations close to the therapeutic doses (Matthews and Boehme, 1988), possibly by targeting endogenous tk or through other unknown mechanisms. We describe here our unexpected finding that GCV is capable of inhibiting proliferation of activated microglia in two disease models with neuroinflammation.

RESULTS AND DISCUSSION

Neuroinflammation in experimental autoimmune encephalomyelitis (EAE) results in an expansion of proliferating microglia

It has been previously reported that microglial activation precedes the infiltration of T cells into the brain parenchyma and clinical symptoms in EAE (Ponomarev et al., 2005; Luo et al., 2007). Indeed, cells expressing the microglia/macrophage marker ionized calcium-binding adaptor molecule 1 (Iba1) show marked proliferation during the active phase of disease (Fig. 1 A) based on its colocalization with the nucleotide analogue BrdU, which marks proliferating cells. This expansion of microglia is seen as early as 7 d postimmunization (d.p.i.; Fig. 1, B and C). Cells expressing Iba1 constituted close to 60% of proliferating cells in the brain, whereas astrocytes expressing glial fibrillary acidic protein (GFAP) or $CD3^+$ T cells showed less proliferation (Fig. 1, A and D; see Fig. 3 A). These results demonstrate that microglia, or recently infiltrated macrophages, undergo a sustained and early expansion in EAE.

GCV attenuates neuroinflammation

We noticed in earlier unrelated studies that the antiviral drug GCV reduced microglial activation (unpublished data); we therefore treated wild-type C57BL/6 mice with GCV or

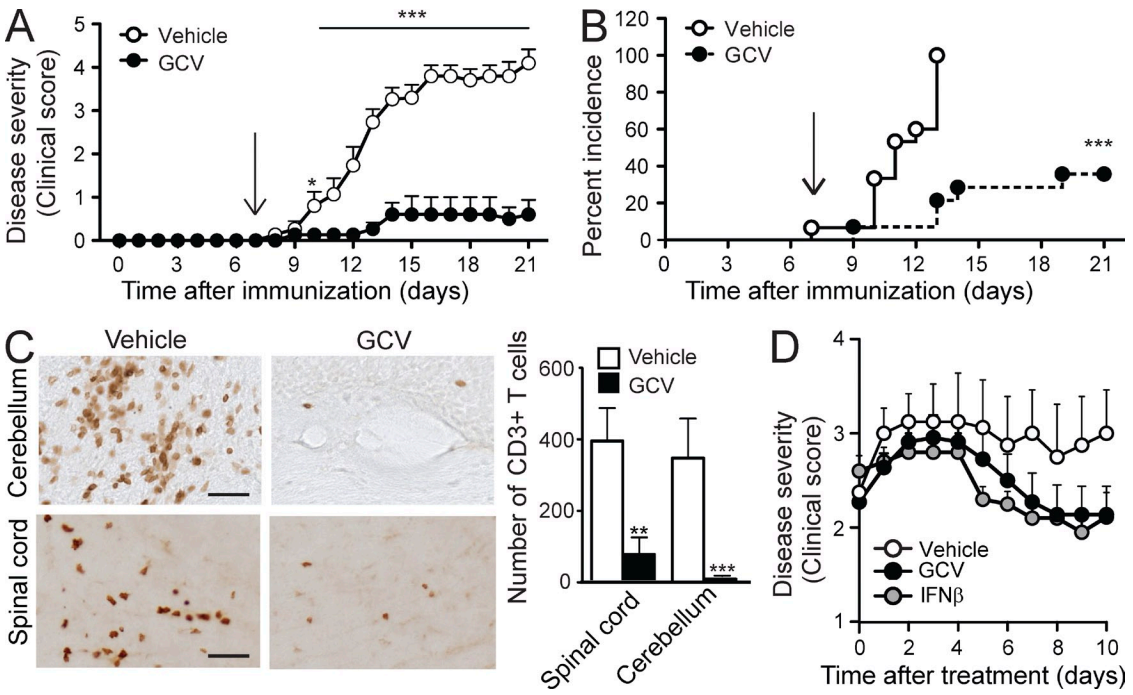

Figure 2. GCV strongly inhibits EAE and neuroinflammation. EAE was induced as in Fig. 1, and mice were treated daily with PBS (vehicle) or 100 mg/kg GCV beginning at 7 d.p.i. (arrows). (A) Disease severity of vehicle- and GCV-treated mice was blindly scored daily. Data represent mean scores and SEM (n = 10–15 mice/group). *, $P < 0.05$; ***, $P < 0.001$ by Mann–Whitney U test. (B) Percent incidence of clinical disease (score > 0) on a given day from A. ***, $P < 0.001$ by Mantel-Cox test. (C) Representative images and quantification of $CD3^+$ T cells in cerebella and spinal cords at 21 d.p.i. from vehicle or GCV-treated mice (bars, 25 µm). Bar graphs represent the mean of three to five sections/mouse and SEM (n = 5–10 mice/group). **, $P < 0.01$; ***, $P < 0.001$ by two-tailed Student's t test. (D) Mice with EAE were treated every alternate day with PBS (vehicle), 100 mg/kg GCV, or 1,000 U IFN-β after the clinical score reached 2. The animals were scored daily, and clinical scores after initiation of treatment are plotted ($P = 0.073$ for GCV and 0.056 for IFN-β, compared with vehicle, by two-way ANOVA). The experiments were independently performed five times for A–C and twice for D.

vehicle starting at 7 d.p.i. Remarkably, although vehicle-treated mice showed robust development of EAE, the disease was almost completely blocked with daily GCV treatment, both in terms of disease severity (Fig. 2 A) and incidence (Fig. 2 B). This effect was mirrored by a >95% reduction in the number of $CD3^+$ T cells in the brain (cerebellum and spinal cord; Fig. 2 C). Additionally, when treatment was started after the EAE mice reached a disease score of 2, GCV-treated mice showed a reduction in disease severity similar to the one conferred by IFN-β (Fig. 2 D; $P = 0.073$ for GCV and $P = 0.056$ for IFN-β by two-way repeated measures ANOVA), which currently is a major treatment for MS patients (Killestein and Polman, 2011) and served here as a positive control (Axtell et al., 2010). However, it's important to note that this approach did not result in a statistically significant reduction in disease. Most importantly, this therapeutic effect of GCV was not dependent on the presence of HSV*tk*, the canonical target of GCV which cleaves this prodrug into a nucleoside analogue (Faulds and Heel, 1990; Culver et al., 1992), and was achieved with an administered dose (100 mg/kg), which is the standard dose used in most mouse virus infection models (Faulds and Heel, 1990) and converts to a human equivalent dose of 8 mg/kg (using conversion factor 12.3 for mouse to human according to FDA guidelines). These doses are thus within the range for GCV used in humans, which can be from 5 mg/kg i.v. twice daily to 1 g three times per day orally.

GCV inhibits microglia proliferation

The amelioration of EAE after GCV treatment was paralleled by strikingly lower numbers of proliferating cells in the brain but not in spleen at 21 d.p.i. (not depicted). GCV treatment specifically reduced the number of proliferating $Iba1^+$ cells, whereas it did not affect the low numbers of proliferating $GFAP^+$ astrocytes or $CD3^+$ T cells at 21 d.p.i. (Fig. 3 A). In addition, the remaining $Iba1^+$ cells in GCV-treated mice appeared smaller and resembled microglia with a ramified, non-activated morphology (Fig. 3 A). To characterize the cellular infiltrates in the CNS of EAE mice and to determine which cell populations were altered by GCV treatment, we used flow cytometry to analyze the mononuclear cells isolated from the CNS at 21 d.p.i. Consistent with histological analysis (Fig. 2 C), GCV treatment led to a significant reduction in frequency (Fig. 3 B, top) and absolute number (not depicted) of $CD4^+$ T cell in the brains. Interestingly, the frequency (Fig. 3 B, middle) and absolute number (not depicted) of $CD11b^+CD45^{hi}$ cells (presumably infiltrated macrophages/activated microglia) in the inflamed CNS were also significantly reduced by GCV treatment, whereas the $CD11b^+CD45^{lo}$ cells (presumably resting microglia) were largely unaltered (not depicted). The majority of the $CD11b^+CD45^{hi}$ cell population was $BrdU^+$, and $BrdU^+CD11b^+CD45^{hi}$ cells were significantly reduced by GCV treatment (Fig. 3 B, bottom). These results

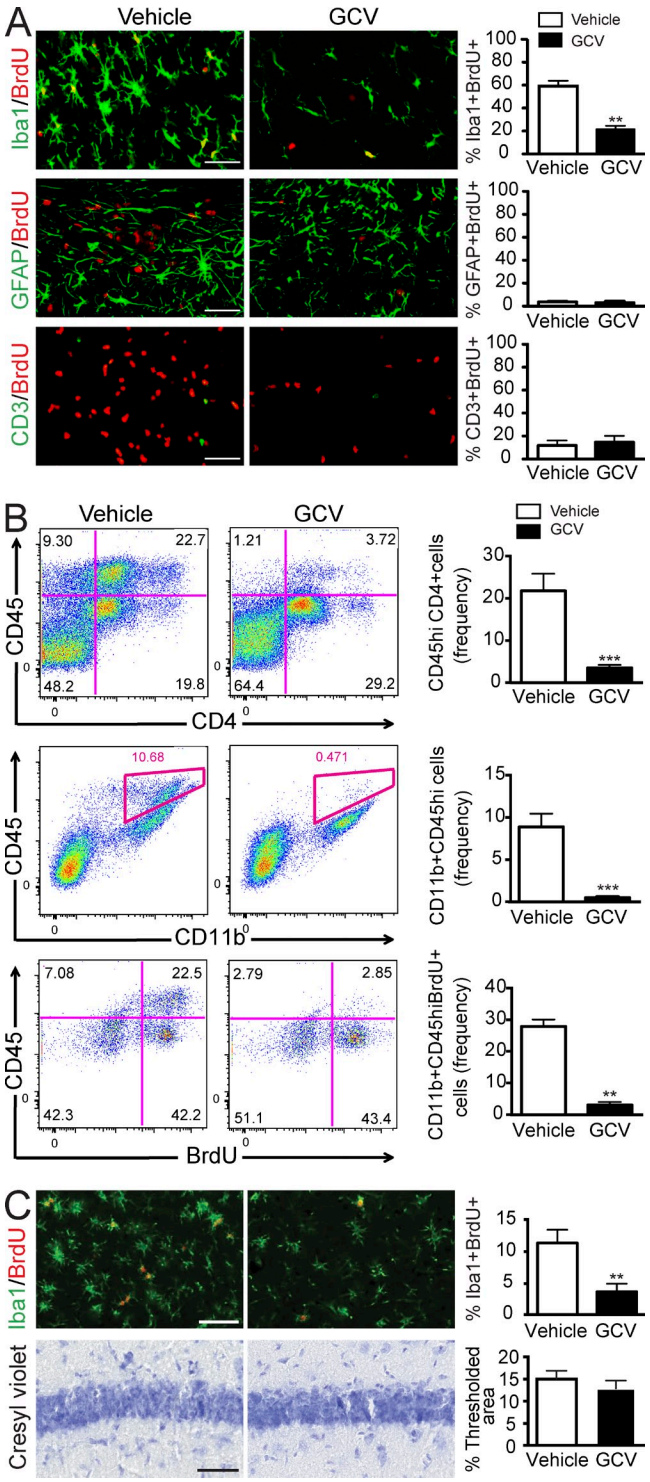

Figure 3. GCV inhibits microglia/macrophage proliferation in the CNS. (A and B) EAE was induced as in Fig. 1, and mice were treated daily with vehicle (PBS) or 100 mg/kg GCV beginning at 7 d.p.i.; BrdU was administered for three consecutive days before sacrifice on 21 d.p.i. (A) Cerebella from vehicle- or GCV-treated EAE mice were double immunolabeled for BrdU and cell type–specific markers Iba1 (microglia), GFAP (astrocytes), and CD3 (T cells). Bar graphs show the mean percentage and SEM of proliferating (BrdU$^+$) microglia (Iba1$^+$), astrocytes (GFAP$^+$), and T cells (CD3$^+$) from three to five sections/animal (n = 5–10 mice/group). (B) Mononuclear cells from cerebellum and spinal cord of vehicle- or GCV-treated EAE mice were enriched by Percoll gradients and analyzed by flow cytometry. Cells were stained with antibodies to BrdU and to cell surface markers CD45, CD11b, CD4, and CD8. (top) Flow cytometry analysis of CD45 and CD4 expression on gated CD8$^-$ cells. Bar graph shows mean ± SEM of percentages of CD45^{hi}CD4$^+$ cells. (middle) Flow cytometry analysis of CD45 and CD11b expression on gated CD8$^-$CD4$^-$ cells. Bar graph shows mean and SEM of percentages of CD45^{hi}CD11b$^+$ cells. (bottom) Flow cytometry analysis of CD45 and BrdU expression on gated CD8$^-$CD4$^-$Cd11b$^+$ cells. Bar graph shows mean and SEM of percentages of CD45^{hi}BrdU$^+$ cells (n = 4 mice/group). **, P < 0.01; ***, P < 0.001 by two-tailed Student's t test. Each experiment was independently performed twice. (C) Mice were injected with kainic acid to induce excitotoxic neurodegeneration and neuroinflammation, and BrdU was injected 1 d before sacrifice on day 5. Coronal sections were stained for Iba1 and BrdU (top) and with cresyl violet (for cell loss; bottom). Bar graphs show mean and SEM from analysis of the hippocampus of three to five sections/animal (n = 5 mice/group). **, P < 0.01 by two-tailed Student's t test. Data shown are representative of two independent experiments. Bars, 50 µm.

suggest that GCV mainly targets proliferating infiltrated macrophage/activated microglia, consistent with a critical role of infiltrating monocytes/macrophages in EAE progression (Ajami et al., 2011).

Furthermore, to determine whether the CNS-specific inhibitory effects of GCV on microglia/macrophages in EAE could be applied to other models, we treated wild-type FvB mice with kainic acid, a glutamate receptor agonist which causes acute excitotoxic neurodegeneration and prominent microglial activation (Luo et al., 2006). 5 d after injury, at the typical readout time in this model, we observed a 75% reduction in the number of BrdU-labeled Iba1-expressing cells in GCV- compared with vehicle-treated mice (Fig. 3 C). GCV treatment did not significantly affect clinical symptoms (seizures, not depicted) or excitotoxic cell death (Fig. 3 C). These findings indicate that the antiproliferative effect of GCV is not limited to EAE but may be a more general outcome and that the roles of proliferating microglia may be different in excitotoxic neurodegeneration and autoimmune inflammation.

GCV does not significantly restrain the peripheral immune response

Treating inflammatory pathology in the CNS without causing general immune suppression is a major challenge in improving therapies for immune-mediated diseases. GCV did not reduce cell proliferation in the spleen of mice with EAE (not depicted), although it had some effects on the distribution of leukocyte subsets in the spleen of these mice (Fig. 4 A). We observed significant increases after GCV treatment in macrophages (CD11b$^+$, CD11c$^-$, CD4/8$^-$) and granulocytes (CD11b$^+$Ly6G^{hi}, CD4/8$^-$) and a decrease in CD4$^+$ T cells and CD4$^+$ dendritic cells (CD11b$^+$CD11c$^+$CD4$^+$) at 21 d.p.i. (Fig. 4 A). Interestingly, arginase-expressing myeloid-derived suppressor cells (MDSCs), which express CD11b$^+$Gr1^{hi}, have been previously shown to promote T lymphocyte apoptosis

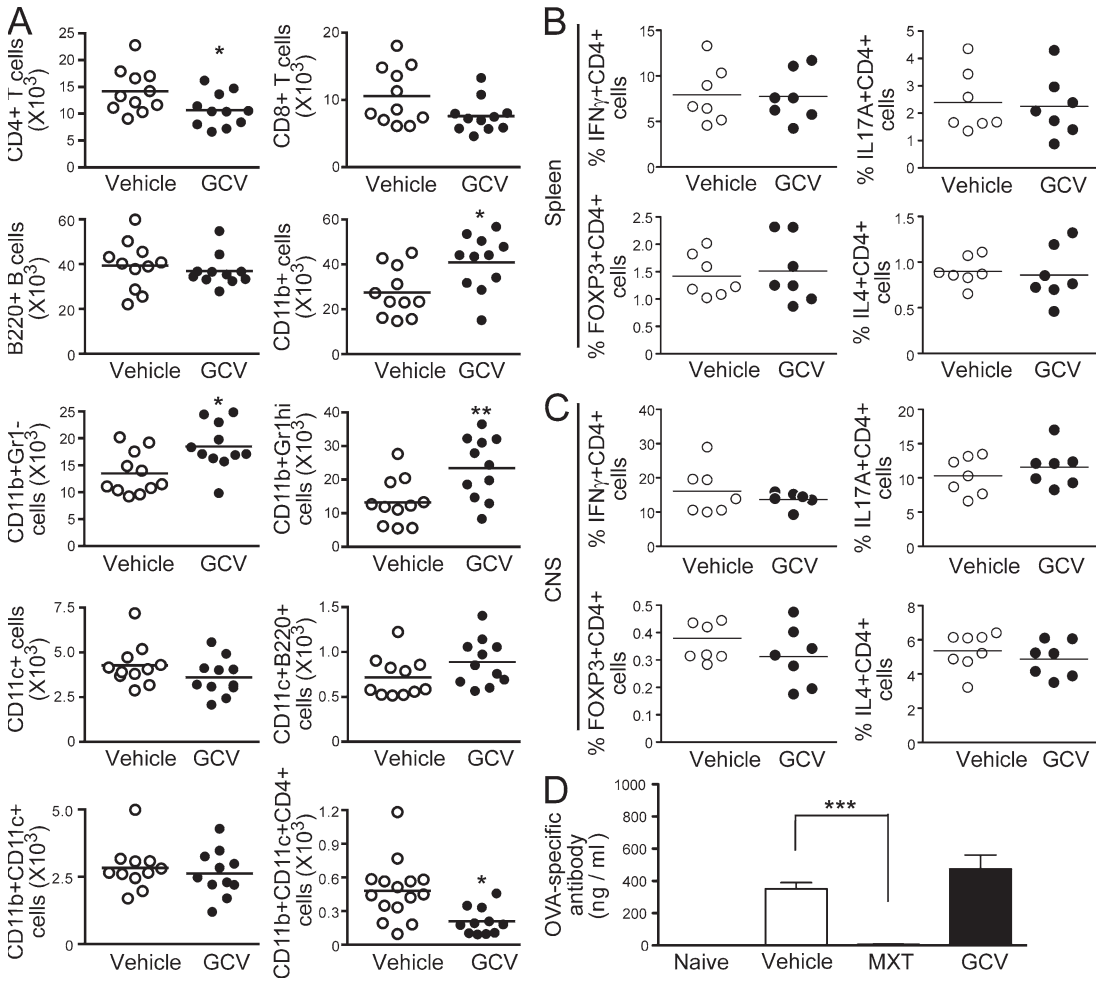

Figure 4. GCV does not alter T cell subset distribution or their ability to mount a systemic immune response. (A–C) EAE was induced as in Fig. 1, and mice were treated daily with vehicle (PBS) or 100 mg/kg GCV beginning at 7 d.p.i. Horizontal bars indicate the mean. (A) Splenocytes were isolated from 21 d.p.i. and stained with the indicated cell type–specific markers. Data represent mean absolute numbers of cells per spleen (n = 11 mice/group). *, $P < 0.05$; **, $P < 0.01$ by two-tailed Student's t test. (B and C) Splenocytes (B) and mononuclear cells from the brain and spinal cord (C) were stimulated with PMA and ionomycin for 5 h, and cells were stained for CD3 and CD4, intracellular cytokines (IL-4, IFN-γ, and IL-17), and the transcription factor (FOXP3). Data represent the percentage of CD4+ T cells that expressed IFN-γ, IL-4, IL-17, and FOXP3 (n = 7 mice/group). (D) 2–3-mo-old naive or OVA_{122}-immunized mice treated daily with vehicle, mitoxantrone, or GCV beginning at 0 d.p.i. were sacrificed at 14 d.p.i. Data represent the mean (±SEM) IgG antibody titer against OVA (n = 5 mice per group). ***, $P < 0.001$ by one-way ANOVA and Dunnett's post-hoc test. Data are representative of three (A–C) or two (D) independent experiments.

and limit neuroinflammation in EAE (Moliné-Velázquez et al., 2011). Likewise, treatment of EAE with Laquinimod was associated with an increase in $CD11b^+Gr1^{hi}$ MDSCs and a reduction in $CD11b^+CD11c^+CD4^+$ cells (Schulze-Topphoff et al., 2012). Therefore, the increased number of $CD11b^+Gr1^{hi}$ cells may contribute, at least in part, to the reduction in peripheral $CD4^+$ T cells and the amelioration of EAE in GCV-treated animals.

To determine whether GCV treatment might affect $CD4^+$ T cell subsets, we performed flow cytometry analysis. GCV had no significant effect on the percentages of $CD4^+$ T cell subsets producing IL-17 (T_H17), IFN-γ (T_H1), or IL4 (T_H2) or expressing $FOXP3^+$ (regulatory T cells [T reg cells]) in the spleen (Fig. 4 B) or the CNS (Fig. 4 C) of mice with EAE.

To determine whether GCV would interfere with a de novo immune response against a foreign antigen in the periphery, we immunized C57BL/6 mice with OVA and treated them concurrently with injections of GCV or vehicle daily for 14 d. Immunized mice treated with vehicle mounted a strong OVA-specific antibody response, which was not reduced by GCV (Fig. 4 D). As a positive control, immunized mice treated with the immunosuppressive drug mitoxantrone, a current treatment option for MS (Hilas et al., 2010), completely abrogated this type of systemic immune response (Fig. 4 D). Together, these findings suggest that GCV has a preferential affinity for proliferating microglia/macrophages in the brain without causing systemic immunosuppression as they occur with conventional immunosuppressive drugs.

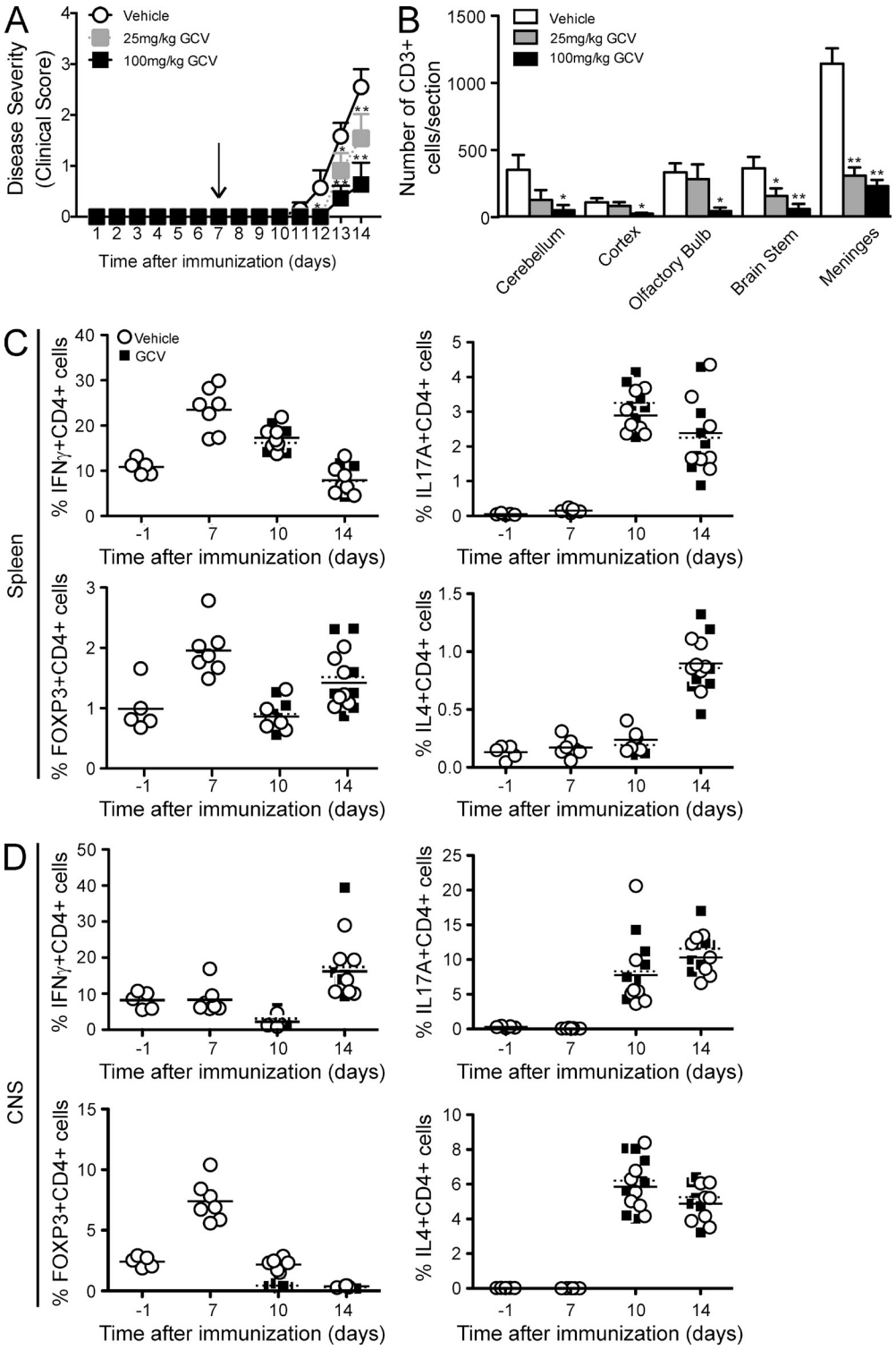

Figure 5. GCV reduces disease severity and T cell infiltration in a dose-dependent manner but does not alter CD4 T cell subsets during the EAE course. (A and B) EAE was induced as in Fig. 1, and mice were sacrificed at 14 d.p.i. Beginning at 7 d.p.i. (arrow), mice were treated daily with vehicle or 25 or 100 mg/kg GCV. Disease severity was scored. Data represent mean scores + SEM (A) and mean + SEM of $CD3^+$ cell numbers counted in various brain regions (B; $n = 5$ mice/group). *, $P < 0.05$; **, $P < 0.01$ by one-way ANOVA followed by Dunnett's test. (C and D) Splenocytes (C) and mononuclear cells from the brain and spinal cord (D) were collected at indicated time points (day −1: naive animals) and stimulated with PMA and ionomycin for 5 h. Cells were stained for CD3 and CD4, intracellular cytokines (IL-4, IFN-γ, and IL-17), and the transcription factor (FOXP3). Data represent the percentage of $CD4^+$ T cells that expressed IFN-γ, IL-4, IL-17, and FOXP3 ($n = 7$ mice per group). Horizontal lines represent the means of the vehicle (solid)- and GCV (dotted)-treated groups. (A–D) Data are representative of two independent experiments.

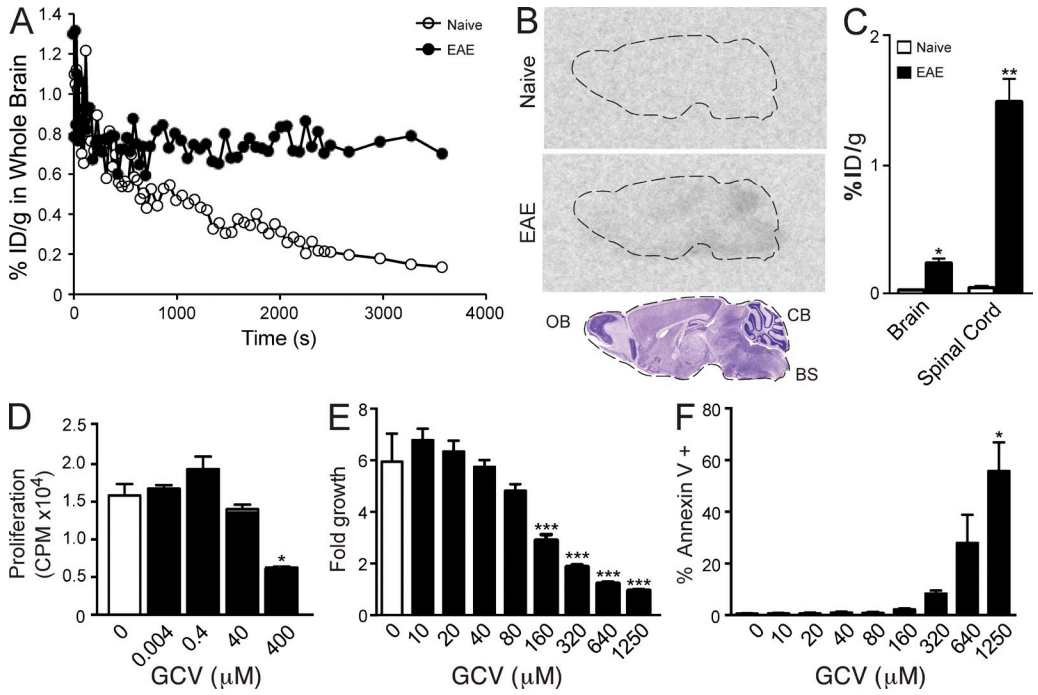

Figure 6. [^{18}F]FHBG accumulates in the CNS of EAE mice and GCV inhibits microglial proliferation in vitro. (A–C) [^{18}F]FHBG was injected i.v. into mice with (mean clinical score = 3) or without (naive) EAE. Acquisition of PET imaging data commenced before [^{18}F]FHBG administration and continued for 60 min. PET images were reconstructed with two-dimensional OSEM and analyzed using AMIDE. (A) Results are expressed as time activity curves depicting the signal of [^{18}F]FHBG in whole mouse brain. (B) Mice were perfused and brains were collected at 60 min after [^{18}F]FHBG injection. Sagittal brain sections (outlined by a dashed line) were cut using a cryostat microtome and exposed to digital autoradiography film. Bottom panel shows schematics of brain sections adapted from the mouse brain atlas (Paxinos and Franklin, 2001) that represent the approximate outline of brain structures. (C) The radioactivity in the tissues was measured with an automated gamma counter and decay-corrected to time of tracer injection. Results are expressed as the percentage of injected dose per gram of tissue (% ID/g). Bar graphs show mean + SEM (n = 3 mice/group). *, $P < 0.05$; **, $P < 0.01$ by Student's t test. Results are from one out of two independent experiments. (D–F) BV-2 mouse microglial cells were treated with the indicated concentrations of GCV and pulsed with [^{3}H]thymidine (D) or assessed for proliferation (E) and apoptosis (F; Annexin V) with Cellavista. Bar graphs show mean + SEM (n = 3 wells/group). *, $P < 0.05$; **, $P < 0.01$; ***, $P < 0.001$ by one-way ANOVA followed by Dunnett's post-test. Each experiment was independently performed at least three times.

GCV attenuates EAE in a dose-dependent manner but does not alter CD4 T cell subsets during the course of EAE

To evaluate the dose-efficacy response of GCV, we treated $MOG_{35–55}$ immunized mice daily with vehicle or 25 or 100 mg/kg GCV starting at 7 d.p.i. GCV reduced disease severity (Fig. 5 A) and T cell infiltration (Fig. 5 B) even at 25 mg/kg, showing a dose-dependent effect at 14 d.p.i. To determine whether GCV may affect T cells during the early phase of disease, we quantified the major T cell subsets in spleen and brain by flow cytometry. As EAE disease progressed, the changes in percentages of each $CD4^+$ T cell subset, T_H17, IFN-γ T_H1, T_H2, or T reg, in these organs followed different patterns (Fig. 5, C and D), but for each of the T cell subsets, GCV-treated animals were indistinguishable from vehicle-treated ones at any time point (Fig. 5, C and D). These findings thus support our earlier observation that GCV treatment does not significantly alter the abundance of CD4 T cell subsets in EAE (Fig. 4, B and C).

GCV and [^{18}F]FHBG accumulate in the brain of EAE animals

We next asked whether GCV might be retained in the CNS and thereby exert localized effects. To explore this possibility, we measured concentrations of GCV in plasma, brain, and spinal cord by liquid chromatography/tandem mass spectrometry. At 21 d.p.i., GCV concentration was four- to five-fold higher in the brain (114 ± 0.038 μg/ml) and spinal cord (0.132 ± 0.014 μg/ml) than in plasma (0.03 ± 0.010 μg/ml) in EAE animals treated with GCV. The concentrations reached in the mouse CNS in our paradigm were therefore three- to sixfold lower than those reached in the CSF of patients treated with 2.5 mg/kg i.v. (0.31–0.68 μg/ml), and mouse plasma concentrations were ∼300-fold lower than the maximal plasma concentration reached in patients after a 1-h dosage regimen (8.27–9.0 μg/ml) with the standard clinical dose of 5 mg/kg i.v. (Genentech, 2010). Furthermore, upon introduction of a radiolabeled analogue of penciclovir (namely, 9-(4-18F-fluoro-3-[hydroxymethyl]butyl)guanine [[^{18}F]FHBG]), which is similar in structure to GCV, we found that [^{18}F]FHBG accumulated and was retained in the brains of EAE animals but not in naive animals (Fig. 6, A–C), suggesting its direct interaction with the inflamed brain.

The aforementioned results open up the possibility that GCV might act directly through microglia in our paradigm. We therefore investigated whether GCV possesses the capacity

to directly inhibit microglial proliferation in cell culture. Using a thymidine incorporation assay (Fig. 6 D) and measurement of cell confluence with an automated cell imaging device (Fig. 6 E), we found that GCV dose-dependently inhibited the proliferation of BV-2 mouse microglial cells in the absence of HSV*tk* and at concentrations that caused no significant cell death (Fig. 6 F). Given that GCV possesses a 1,000-fold higher affinity for HSV*tk* over endogenous cellular tk (Matthews and Boehme, 1988), it is conceivable that GCV targets activated microglia at least in part through a mechanism independent of endogenous tk. Together, our results demonstrate that GCV is capable of inhibiting the proliferation of activated microglia in vivo and in vitro.

Our results demonstrate that GCV inhibits the proliferation of activated CNS-resident microglia or infiltrating macrophages independent of HSV*tk*, whereas it does not significantly inhibit the proliferation of astrocytes or T cells infiltrating the brain. They further highlight the role of microglia in neuroinflammatory disorders and support microglia as a potential treatment target. Our results are in line with studies showing that the main therapeutic effects of IFN-β in MS are mediated through microglia/macrophages (Prinz et al., 2008) and that functional inhibition of microglia reduces clinical symptoms in EAE (Ponomarev et al., 2011; Saijo et al., 2011). Likewise, ablation of CNS-resident microglia reduced EAE in GCV-treated transgenic mice expressing HSV*tk* in the macrophage lineage (Heppner et al., 2005). However, in this genetically engineered model, GCV causes deletion of all HSV*tk*-expressing cells, leading to hematopoietic toxicity and necessitating the transfer of wild-type bone marrow into lethally irradiated transgenic mice. Using this transfer paradigm and dosing every 2 d, GCV did not affect EAE severity in nontransgenic control mice. In contrast, we discovered that activated microglia in wild-type mice with EAE were susceptible to inhibition by GCV alone (daily dosing), in the absence of HSV*tk*, at doses equivalent to the ones used to treat humans with viral infections (25 or 100 mg/kg body weight). These unexpected effects may be the result of a combination of higher doses of GCV used in our study and microglia's unique ability to rejuvenate independent of the bone marrow (Geissmann et al., 2010; Ajami et al., 2011) or to proliferate in the specialized environment present in the inflamed brain. We also noted a selective accumulation of GCV in the inflamed brain and spinal cord of mice with EAE, suggesting its direct involvement in the modulation of microglia.

The mechanism by which GCV inhibits the proliferation of activated wild-type microglia remains unclear. The mice used here were negative for HSV-related virus MuHV-4 (not depicted), and we could not find any viral tk-related sequences in the mouse (or human) genome, supporting the possibility that GCV acts independently of viral tk in these cells. But it remains a possibility that EAE depends on immune-mediated bystander activation of an unknown virus and that GCV acts as an antiviral agent. Whether GCV or its analogues may have therapeutic effects in humans remains to be seen, but encouragingly, a stabilizing and statistically significant effect in a clinical study with acyclovir was detected in relapsing/remitting MS patients when comparing patients with their individual baseline (Lycke et al., 1996). However, only trends of improvements were detected in clinical studies of MS with valacyclovir (converted to acyclovir upon ingestion; Bech et al., 2002; Friedman et al., 2005). Altogether, our results identify GCV as a potential novel therapeutic for neurological diseases associated with microglial proliferation and neuroinflammation.

MATERIAL AND METHODS

Mice. We obtained all C57BL/6 and FvB mice from the Jackson Laboratory. Mice were between 8 and 12 wk of age when experiments were initiated. Animal handling was performed in accordance with institutional guidelines and approved by the Institutional Animal Care and Use Committee of the Veterans Affair Palo Alto Health Care System.

EAE induction and assessment. $MOG_{35–55}$ peptide (MEVGWYRSPFSRVVH-LYRNGK) was synthesized by the Stanford Protein and Nucleic Acid Biotechnology Facility and purified by high-performance liquid chromatography to >95% purity. Mice (8–12 wk old) were immunized subcutaneously with a total of 200 µg $MOG_{35–55}$ peptide emulsified in CFA (200 µg mycobacterium tuberculosis; Difco adjuvants; BD) and received an i.v. injection of 400 ng pertussis toxin (List Biological Laboratories, Inc.) at the time of immunization and 48 h later. Mice were weighed and examined daily for clinical signs of EAE and scored as previously described (Luo et al., 2007): 0, no paralysis; 1, loss of tail tone; 2, hind limb weakness or paresis; 3, hind limb paralysis; 4, hind limb paralysis and forelimb paresis; 5, moribund or dead. 50 mg/kg BrdU was injected intraperitoneally for 3 d before sacrifice to label dividing cells.

Kainic acid administration. Kainic acid (Tocris Bioscience) was dissolved in PBS and injected subcutaneously (20 mg/kg) in mice (Luo et al., 2006). Mice were then weighed and examined daily for clinical signs of seizures.

GCV, IFN-β, and mitoxantrone treatments. Clinical grade GCV/Cytovene (Roche) was obtained as a lyophilized powder and reconstituted in deionized water before use. The drug was administered daily via intraperitoneal injections at 25 or 100 mg/kg body weight. In some experiments, 100 mg/kg GCV, 1,000 U/dose of recombinant mouse IFN-β (PBL Interferon Source; Axtell et al., 2010), or PBS was given intraperitoneally every other day after the mice reached a clinical score of 2 or more. 0.5 mg/kg mitoxantrone (Teva Parenteral Medicine) was administered intraperitoneally daily as described previously (Lublin et al., 1987). Mice were scored daily starting at 7 d.p.i.

Tissue preparation. Mice were anesthetized with 400 mg/kg chloral hydrate (Sigma-Aldrich) before removal of the spleen, which was dissected in halves and weighed. Mice were then transcardially perfused with 0.9% saline, followed by the removal of the spinal cord and brain, which were dissected into two hemibrains. One half of the spleen, a hemibrain and the entire spinal cord were fixed for 24 h in 4% paraformaldehyde and cryoprotected in 30% sucrose. Brains were sectioned sagittally at 40 µm, whereas the spleens were sectioned transversally at 40 µm using a freezing microtome (Leica) and stored in cryoprotective medium at −20°C (Luo et al., 2006, 2007). The other half of brain and spleen were then processed for cell isolation.

Cell isolation from spleen and CNS tissue. Spleens and brains were dissociated by grinding through 100-µM cell strainers and suspended in RPMI-1640 with 10% FBS (RP10) or HBSS, respectively. To obtain a single-cell suspension, dissociated brain cells in HBSS were digested with 300 U/ml clostridial collagenase (type V; Roche) and 50 µg/ml DNaseI (Sigma-Aldrich) for 1 h at 37°C with mild agitation and halted with the addition of RP10. The brain cells were then washed with HBSS and resuspended in 30%

Percoll (GE Healthcare), followed by an underlay of 70% Percoll and overlay of 10% Percoll. This Percoll gradient was then centrifuged at 500 *g* for 20 min at 4°C with the brakes off. Myelin debris was removed from the 10% Percoll layer, and mononuclear cells were collected from the 30%/70% interface and resuspended with RP10 for further flow cytometry analysis (Luo et al., 2007).

Immunohistochemistry. Immunohistochemistry was performed on free-floating sections according to standard procedures (Luo et al., 2007). Primary antibodies were against BrdU (1:2,000; Abcam), GFAP (1:1,000; Dako), Iba1 (1:1,000; Wako Chemicals USA), and CD3 (1:1,000; BD). Before addition of primary antibody against BrdU, sections were treated in 3M HCl for 30 min at 37°C for antigen retrieval. Primary antibody staining was revealed using biotinylated secondary antibodies and the ABC kit (Vector Laboratories) with diaminobenzidine (DAB; Sigma-Aldrich). For double-immunolabeling, we used secondary antibodies conjugated to fluorophores (Alexa Fluor 644, Cy5 at 1:2,000; Invitrogen) against the animal primary antibodies were raised in. Staining was performed on three to five sections per animal and quantified by counting the number of positive stained cells. Light microscopy was performed with a CoolSNAP HQ camera (Photometrics) mounted on an IX71 microscope (Olympus). For confocal microscopy, we used an LSM510 META confocal microscope (Carl Zeiss).

Flow cytometry analysis. At various time points after EAE induction (including naive), isolated brain and spleen cells were stained with cell surface makers in FACS buffer (PBS, 1% FBS, and 0.2% NaAz) to determine the abundance of various cell types: CD11b (M1/70; BD) for macrophages, CD11c (N418; eBioscience) for dendritic cells, B220 (RA3-6B2; BD) for B cells, Ly6G (RB6-8L5; eBioscience) for neutrophils, CD4 (GK1.5; BD) for $CD4^+$ T cells, and CD8 (53-6.7; BD) for $CD8^+$ T cells. To determine subsets of $CD4^+$ T cells, isolated brain and spleen cells were stimulated with 50 ng/ml PMA and 1 µg/ml ionomycin for 5 h, with the addition of GolgiStop (brefeldin A; BD) after 2 h to inhibit the secretion of vesicles containing cytokines. Intracellular cytokine and BrdU stainings were then performed according to BD's Cytofix/Cytoperm and BrdU protocols, respectively. The following antibodies were used to detect BrdU (PRB-1; eBioscience), FOXP3 (FJK-1ba; eBioscience), IFN-γ (XMG1.2; eBioscience), IL-4 (BVD6-24G2; eBioscience), and IL-17A (eBio17B7; eBioscience).

Proliferation assay. To assess cell proliferation by thymidine incorporation, a total of 2×10^4 BV-2 cells were seeded in a 96-well plate for a maximum of 12 h in 10% FBS containing DMEM and then serum starved for an additional 12 h before the addition of varying concentrations of GCV for a total of 24 h. Cultures were pulsed for the final 8 h with 1 µCi/well [^{3}H]thymidine (GE Healthcare) before incorporated radioactivity was measured using a β plate scintillation counter (Luo et al., 2007).

In a second, independent proliferation assay, BV-2 cells were seeded at 2,000 cells/well in 96-well plates and incubated overnight. GCV was added at the indicated concentrations, and percent confluence was measured with a Cellavista automated image reader (Roche) at 48 h after GCV addition. Percent confluence was normalized to the respective 0-h percent confluence and is plotted as fold growth. Apoptosis was measured by staining GCV-treated BV-2 cells with Annexin V-FITC.

OVA immunization and measurement of antibody responses. Mice were immunized subcutaneously with 100 µg OVA (Sigma-Aldrich) emulsified in an equal volume of CFA. Two subcutaneous injections were administered near each armpit (50 µg/injection). 1 d before and 14 d after immunization, plasma was collected to analyze basal (−1 d) and peak (14 d) OVA-specific antibody responses. OVA-specific antibodies were quantified using ELISA. In brief, flat-bottom 96-well RIA plates (Costar) were coated with 100 µg/ml OVA in PBS + 0.02% sodium azide. Plates were incubated for 2 h at 37°C, washed with PBS, and blocked overnight at 4°C with PBS + 1% BSA. Plates were washed with PBS + 0.05% Tween. After the wash, 100 µl of diluted plasma (to create a dilution curve) or mouse anti-OVA IgG_1 (Sigma-Aldrich; to create a standard curve) was incubated in the appropriate well for 2 h at 37°C. Plates were then washed with PBS + 0.05% Tween and incubated with alkaline phosphatase–conjugated goat anti–mouse IgG antibody (Sigma-Aldrich; diluted 1:1,000 in PBS + 1% BSA) for 2 h at 37°C. Plates were washed with PBS + 0.05% Tween, followed by PBS, and then bound antibodies were visualized by incubating with 1 µg/ml p-nitrophenyl phosphate in 10 mM diethanolamine–0.5 mM $MgCl_2$ buffer (Sigma-Aldrich). Spectrophotometric readings were performed on a SpectraMax microplate reader (Molecular Devices) at a wavelength of 405 nm.

[^{18}F]FHBG PET imaging, ex vivo autoradiography, and biodistribution. [^{18}F]FHBG was synthesized via nucleophilic aliphatic substitution using previously reported procedures (Chin et al., 2008) in a commercially available, automated module. PET imaging was performed on a microPET R4 model scanner (Siemens) fitted with a computer-controlled bed, 10.8-cm transaxial and 8-cm axial field of view (FOV), and no septa and operated exclusively in three-dimensional list mode. PET images were reconstructed with two-dimensional OSEM (ordered subsets expectation maximization) and analyzed using AMIDE (a medical image data examiner; Loening and Gambhir, 2003). Naive and EAE mice (20–30 g) were anaesthetized using isoflurane (2% for induction and 1–3% for maintenance). Acquisition of the PET data in list mode was commenced before i.v. administration of [^{18}F]FHBG (120–150 µCi in 100 µl of 0.9% saline) via the tail vein and was continued for a period of 60 min. Immediately after PET imaging, each mouse was perfused with 20 ml saline to remove blood from the brain. Organs (brain and spinal cord) were quickly removed, weighed, and placed in tubes for gamma counting. Radioactivity in weighed organs was assessed via an automated gamma counter and decay-corrected to time of tracer injection using diluted aliquots of the initial administered dose as standards. For autoradiography, 12-µm-thick sagittal brain sections were cut using a cryostat microtome HM500 (Microm). The sections were mounted on microscope slides (Fisherbrand Superfrost Plus; Thermo Fisher Scientific), air-dried for 10 min, and then exposed to ^{18}F-sensitive storage phosphor screens (PerkinElmer) for 12 h at 4°C. The image plates were analyzed using a Typhoon 9410 Variable Mode Imager (GE Healthcare), and image data were visualized and processed by ImageJ (National Institutes of Health).

Statistics. All statistical analysis was computed using Prism (GraphPad Software). Differences between treatment conditions were established using unpaired Student's *t* test (with two conditions) or ANOVA followed by Dunnett's or Tukey's post-test for multiple comparisons (for more than two conditions). EAE clinical score and percent incidence data were statistically evaluated using Mann–Whitney and Log-rank (Mantel-Cox) tests, respectively. P-values of <0.05 were considered significant. Statistic details are indicated in the respective figure legends.

We thank all members of the Wyss-Coray laboratory for helpful discussions. Additionally, we thank S.A. Villeda for insightful comments.

This work was supported by grants from the National Institutes of Health (R01 AG27505 to T. Wyss-Coray; T32 AI07290 and F31 NS066676 to Z. Ding) and the Department of Veterans Affairs.

The authors declare no competing financial interests.

Author contributions: T. Wyss-Coray, Z. Ding, J. Luo, L. Steinman, and S.S. Gambhir conceived the experiments. Z. Ding and J. Luo performed the EAE experiments. Z. Ding and K.M. Lucin performed the OVA immunization and OVA antibody ELISA. Z. Ding, V. Mathur, and P.P. Ho performed the proliferation assays. Z. Ding performed the immunohistochemistry and flow cytometry. H. Alabsi performed the quantification of BrdU and CD3 immunohistochemistry. Z. Ding, M.L. James, A. Hoehne, and V. Mathur performed the [^{18}F]FHBG experiments. Z. Ding, J. Luo, and T. Wyss-Coray wrote the manuscript.

Submitted: 30 March 2012
Accepted: 10 January 2014

REFERENCES

Ajami, B., J.L. Bennett, C. Krieger, K.M. McNagny, and F.M. Rossi. 2011. Infiltrating monocytes trigger EAE progression, but do not contribute to the resident microglia pool. *Nat. Neurosci.* 14:1142–1149. http://dx.doi.org/10.1038/nn.2887

Axtell, R.C., B.A. de Jong, K. Boniface, L.F. van der Voort, R. Bhat, P. De Sarno, R. Naves, M. Han, F. Zhong, J.G. Castellanos, et al. 2010. T helper type 1 and 17 cells determine efficacy of interferon-beta in multiple sclerosis and experimental encephalomyelitis. *Nat. Med.* 16:406–412. http://dx.doi.org/10.1038/nm.2110

Banati, R.B., J. Newcombe, R.N. Gunn, A. Cagnin, F. Turkheimer, F. Heppner, G. Price, F. Wegner, G. Giovannoni, D.H. Miller, et al. 2000. The peripheral benzodiazepine binding site in the brain in multiple sclerosis: quantitative in vivo imaging of microglia as a measure of disease activity. *Brain*. 123:2321–2337. http://dx.doi.org/10.1093/brain/123.11.2321

Bech, E., J. Lycke, P. Gadeberg, H.J. Hansen, C. Malmeström, O. Andersen, T. Christensen, S. Ekholm, S. Haahr, P. Höllsberg, et al. 2002. A randomized, double-blind, placebo-controlled MRI study of anti-herpes virus therapy in MS. *Neurology*. 58:31–36. http://dx.doi.org/10.1212/WNL.58.1.31

Bhaskar, K., M. Konerth, O.N. Kokiko-Cochran, A. Cardona, R.M. Ransohoff, and B.T. Lamb. 2010. Regulation of tau pathology by the microglial fractalkine receptor. *Neuron*. 68:19–31. http://dx.doi.org/10.1016/j.neuron.2010.08.023

Boillée, S., K. Yamanaka, C.S. Lobsiger, N.G. Copeland, N.A. Jenkins, G. Kassiotis, G. Kollias, and D.W. Cleveland. 2006. Onset and progression in inherited ALS determined by motor neurons and microglia. *Science*. 312:1389–1392. http://dx.doi.org/10.1126/science.1123511

Chin, F.T., M. Namavari, J. Levi, M. Subbarayan, P. Ray, X. Chen, and S.S. Gambhir. 2008. Semiautomated radiosynthesis and biological evaluation of [18F]FEAU: a novel PET imaging agent for HSV1-tk/sr39tk reporter gene expression. *Mol. Imaging Biol.* 10:82–91. http://dx.doi.org/10.1007/s11307-007-0122-3

Culver, K.W., Z. Ram, S. Wallbridge, H. Ishii, E.H. Oldfield, and R.M. Blaese. 1992. In vivo gene transfer with retroviral vector-producer cells for treatment of experimental brain tumors. *Science*. 256:1550–1552. http://dx.doi.org/10.1126/science.1317968

Faulds, D., and R.C. Heel. 1990. Ganciclovir. A review of its antiviral activity, pharmacokinetic properties and therapeutic efficacy in cytomegalovirus infections. *Drugs*. 39:597–638. http://dx.doi.org/10.2165/00003495-199039040-00008

Fillat, C., M. Carrió, A. Cascante, and B. Sangro. 2003. Suicide gene therapy mediated by the Herpes Simplex virus thymidine kinase gene/Ganciclovir system: fifteen years of application. *Curr. Gene Ther.* 3:13–26. http://dx.doi.org/10.2174/1566523033347426

Friedman, J.E., J.B. Zabriskie, C. Plank, D. Ablashi, J. Whitman, B. Shahan, R. Edgell, M. Shieh, O. Rapalino, R. Zimmerman, and D. Sheng. 2005. A randomized clinical trial of valacyclovir in multiple sclerosis. *Mult. Scler.* 11:286–295. http://dx.doi.org/10.1191/1352458505ms1185oa

Geissmann, F., M.G. Manz, S. Jung, M.H. Sieweke, M. Merad, and K. Ley. 2010. Development of monocytes, macrophages, and dendritic cells. *Science*. 327:656–661. http://dx.doi.org/10.1126/science.1178331

Genentech. 2010. Cytovene-IV (Ganciclovir Sodium for Injection) for Intravenous Infusion Only. Genentech, South San Francisco, CA. http://www.gene.com/download/pdf/cytovene_prescribing.pdf (accessed October 15, 2013).

Heppner, F.L., M. Greter, D. Marino, J. Falsig, G. Raivich, N. Hövelmeyer, A. Waisman, T. Rülicke, M. Prinz, J. Priller, et al. 2005. Experimental autoimmune encephalomyelitis repressed by microglial paralysis. *Nat. Med.* 11:146–152. http://dx.doi.org/10.1038/nm1177

Hilas, O., P.N. Patel, and S. Lam. 2010. Disease modifying agents for multiple sclerosis. *Open Neurol J.* 4:15–24. http://dx.doi.org/10.2174/1874205X01004010015

Killestein, J., and C.H. Polman. 2011. Determinants of interferon β efficacy in patients with multiple sclerosis. *Nat Rev Neurol.* 7:221–228. http://dx.doi.org/10.1038/nrneurol.2011.22

Loening, A.M., and S.S. Gambhir. 2003. AMIDE: a free software tool for multimodality medical image analysis. *Mol. Imaging*. 2:131–137. http://dx.doi.org/10.1162/153535003322556877

Lublin, F.D., M. Lavasa, C. Viti, and R.L. Knobler. 1987. Suppression of acute and relapsing experimental allergic encephalomyelitis with mitoxantrone. *Clin. Immunol. Immunopathol.* 45:122–128. http://dx.doi.org/10.1016/0090-1229(87)90118-8

Lucin, K.M., and T. Wyss-Coray. 2009. Immune activation in brain aging and neurodegeneration: too much or too little? *Neuron*. 64:110–122. http://dx.doi.org/10.1016/j.neuron.2009.08.039

Luo, J., A.H. Lin, E. Masliah, and T. Wyss-Coray. 2006. Bioluminescence imaging of Smad signaling in living mice shows correlation with excitotoxic neurodegeneration. *Proc. Natl. Acad. Sci. USA*. 103:18326–18331. http://dx.doi.org/10.1073/pnas.0605077103

Luo, J., P.P. Ho, M.S. Buckwalter, T. Hsu, L.Y. Lee, H. Zhang, D.K. Kim, S.J. Kim, S.S. Gambhir, L. Steinman, and T. Wyss-Coray. 2007. Glia-dependent TGF-beta signaling, acting independently of the TH17 pathway, is critical for initiation of murine autoimmune encephalomyelitis. *J. Clin. Invest.* 117:3306–3315. http://dx.doi.org/10.1172/JCI31763

Lycke, J., B. Svennerholm, E. Hjelmquist, L. Frisén, G. Badr, M. Andersson, A. Vahlne, and O. Andersen. 1996. Acyclovir treatment of relapsing-remitting multiple sclerosis. A randomized, placebo-controlled, double-blind study. *J. Neurol.* 243:214–224. http://dx.doi.org/10.1007/BF00868517

Matthews, T., and R. Boehme. 1988. Antiviral activity and mechanism of action of ganciclovir. *Rev. Infect. Dis.* 10:S490–S494. http://dx.doi.org/10.1093/clinids/10.Supplement_3.S490

Min, J.J., M. Iyer, and S.S. Gambhir. 2003. Comparison of [18F]FHBG and [14C]FIAU for imaging of HSV1-tk reporter gene expression: adenoviral infection vs stable transfection. *Eur. J. Nucl. Med. Mol. Imaging*. 30:1547–1560. http://dx.doi.org/10.1007/s00259-003-1238-6

Moliné-Velázquez, V., H. Cuervo, V. Vila-Del Sol, M.C. Ortega, D. Clemente, and F. de Castro. 2011. Myeloid-derived suppressor cells limit the inflammation by promoting T lymphocyte apoptosis in the spinal cord of a murine model of multiple sclerosis. *Brain Pathol.* 21:678–691. http://dx.doi.org/10.1111/j.1750-3639.2011.00495.x

Paxinos, G., and K.B.J. Franklin. 2001. The Mouse Brain in Stereotaxic Coordinates. Second edition. Academic Press, San Diego. 296 pp.

Ponomarev, E.D., L.P. Shriver, K. Maresz, and B.N. Dittel. 2005. Microglial cell activation and proliferation precedes the onset of CNS autoimmunity. *J. Neurosci. Res.* 81:374–389. http://dx.doi.org/10.1002/jnr.20488

Ponomarev, E.D., T. Veremeyko, N. Barteneva, A.M. Krichevsky, and H.L. Weiner. 2011. MicroRNA-124 promotes microglia quiescence and suppresses EAE by deactivating macrophages via the C/EBP-α-PU.1 pathway. *Nat. Med.* 17:64–70. http://dx.doi.org/10.1038/nm.2266

Prinz, M., H. Schmidt, A. Mildner, K.P. Knobeloch, U.K. Hanisch, J. Raasch, D. Merkler, C. Detje, I. Gutcher, J. Mages, et al. 2008. Distinct and nonredundant in vivo functions of IFNAR on myeloid cells limit autoimmunity in the central nervous system. *Immunity*. 28:675–686. http://dx.doi.org/10.1016/j.immuni.2008.03.011

Saijo, K., and C.K. Glass. 2011. Microglial cell origin and phenotypes in health and disease. *Nat. Rev. Immunol.* 11:775–787. http://dx.doi.org/10.1038/nri3086

Saijo, K., J.G. Collier, A.C. Li, J.A. Katzenellenbogen, and C.K. Glass. 2011. An ADIOL-ERβ-CtBP transrepression pathway negatively regulates microglia-mediated inflammation. *Cell*. 145:584–595. http://dx.doi.org/10.1016/j.cell.2011.03.050

Schulze-Topphoff, U., A. Shetty, M. Varrin-Doyer, N. Molnarfi, S.A. Sagan, R.A. Sobel, P.A. Nelson, and S.S. Zamvil. 2012. Laquinimod, a quinoline-3-carboxamide, induces type II myeloid cells that modulate central nervous system autoimmunity. *PLoS ONE*. 7:e33797. http://dx.doi.org/10.1371/journal.pone.0033797